



**HAL**  
open science

## TeO<sub>2</sub>-ZnO-La<sub>2</sub>O<sub>3</sub> tellurite glass system investigation for mid-infrared robust optical fibers manufacturing

A. Maldonado, M. Evrard, E. Serrano, A. Crochetet, F. Désévéday, J.C. Jules, G. Gadret, C.H. Brachais, C. Strutynski, Y. Ledemi, et al.

### ► To cite this version:

A. Maldonado, M. Evrard, E. Serrano, A. Crochetet, F. Désévéday, et al.. TeO<sub>2</sub>-ZnO-La<sub>2</sub>O<sub>3</sub> tellurite glass system investigation for mid-infrared robust optical fibers manufacturing. *Journal of Alloys and Compounds*, 2021, 867, pp.159042. 10.1016/j.jallcom.2021.159042 . hal-03544589

**HAL Id: hal-03544589**

**<https://hal.science/hal-03544589>**

Submitted on 13 Feb 2023

**HAL** is a multi-disciplinary open access archive for the deposit and dissemination of scientific research documents, whether they are published or not. The documents may come from teaching and research institutions in France or abroad, or from public or private research centers.

L'archive ouverte pluridisciplinaire **HAL**, est destinée au dépôt et à la diffusion de documents scientifiques de niveau recherche, publiés ou non, émanant des établissements d'enseignement et de recherche français ou étrangers, des laboratoires publics ou privés.



Distributed under a Creative Commons Attribution - NonCommercial 4.0 International License

# TeO<sub>2</sub> – ZnO - La<sub>2</sub>O<sub>3</sub> tellurite glass system investigation for mid infrared robust optical fibers manufacturing

A. Maldonado<sup>a, b</sup>, M. Evrard<sup>a</sup>, E. Serrano<sup>a</sup>, A. Crochetet<sup>a</sup>, F. Désévéday<sup>a</sup>, J.C. Jules<sup>a</sup>, G. Gadret<sup>a</sup>, C.H. Brachais<sup>a</sup>, C. Strutynski<sup>a</sup>, Y. Ledemi<sup>b</sup>, Y. Messaddeq<sup>b</sup>, F. Smektala<sup>a, \*</sup>

<sup>a</sup> *Laboratoire Interdisciplinaire Carnot de Bourgogne, UMR 6303 CNRS-Université de Bourgogne Franche-Comté, 9 avenue Alain Savary, 21078 Dijon, France*

<sup>b</sup> *Centre d'Optique, Photonique et Laser, Université Laval, 2375 rue de la Terrasse, Québec (QC), G1V 0A6, Canada*

\*frederic.smektala@u-bourgogne.fr

## Abstract

TeO<sub>2</sub>-ZnO-La<sub>2</sub>O<sub>3</sub> (TZL) ternary glasses were investigated in order to manufacture step-index optical fibers with low optical losses in the near- and mid-infrared ranges and superior mechanical properties. To identify appropriate TZL glass compositions for optical fibers manufacturing, the whole vitreous domain of the ternary diagram was explored by characterizing bulk samples from thermal and optical point of view. Investigations were focused on understanding how the refractive index evolves as a function of the composition. For this, several parameters were analyzed such as density, molar volume, oxygen packing density, molar refractivity, polarizability and optical basicity. **Finally, thermal and structural studies such as DSC and X-Ray diffraction allowed to select the most promising core and cladding glasses combination (in terms of stability against crystallization), in order to draw optical fibers.** Step-index optical fibers were then successfully fabricated. Optical losses of these first TZL fibers were measured, giving minimum attenuations of 1.25dB/m at 2.15μm and less than 2dB/m up to 2.75μm and compared to well-known TeO<sub>2</sub> - ZnO – Na<sub>2</sub>O (TZN) glass fibers. Finally, first mechanical tests were performed as microhardness and tensile strength measurements with the aim of demonstrating the improvement in workability and resistance of the TZL fibers compared to TZN fibers.

## Keywords

Lanthanum tellurite glasses, Mid infrared, Optical fibers, Step-index, Fiber manufacturing

## 1. Introduction

Tellurite glasses exhibit unique properties that offer promising perspectives for many applications in various fields such as telecommunication, defense, environment, medicine and so on. These glasses are transparent from the visible to the mid-infrared (~6.5 μm) range and show high linear and nonlinear refractive indices (up to 20 times higher than silicate glasses) which allow their use in several infrared optical applications [1, 2]. Furthermore, they present an interesting corrosion resistance intermediate to fluoride and silica [3], high rare earth solubility (up to 19 mol% in erbium-doped fluorotellurite glasses according to Wang *et al.* [4]) and exhibit a huge range of possible chemical compositions which enables to envisage many possible glass compositions depending on the intended application.

In several of our reported works, tellurite glasses have been used to design step-index optical fibers for supercontinuum light generation applications [5] or multimaterial glass-metal optical fibers to combine the transport of electrical pulses with broadband mid-infrared optical signals [6]. All these studies were relying on the well-known TZN vitreous system, in particular the **TZN 80-10-10 (80TeO<sub>2</sub> – 10ZnO – 10Na<sub>2</sub>O (in mol.%))** glass composition ( $T_g = 285^\circ\text{C}$ ). Such glass transition temperature ( $T_g$ ) has a disadvantage in the case of multimaterial fibers when selecting a thermally compatible metal alloy for co-drawing. Thus, we have oriented our investigations on alkali-free tellurite glass compositions offering higher  $T_g$  as well as lower optical attenuation. To this purpose, we replaced sodium oxide Na<sub>2</sub>O in the TZN system by lanthanum oxide La<sub>2</sub>O<sub>3</sub>, to form TeO<sub>2</sub> – ZnO – La<sub>2</sub>O<sub>3</sub> (TZL) compositions which combine these two properties according to Rhonehouse's works [3, 7] and present also a high corrosion resistance as well as a low absorption in the UV-visible and mid-infrared. Indeed, the substitution of sodium oxide for rare earth oxide such as La<sub>2</sub>O<sub>3</sub> into tellurite glass network increases its stability against crystallization as well as its  $T_g$  by taking advantage of its high melting temperature (2315°C) [8, 9]. **Thus, the absence of alkali (mainly sodium) helps to limit the number of non-bridging oxygens in the network as well as the basicity of the glass melt, thus decreasing reactivity with water so OH contamination in the glass which is a source of unwanted absorption and heating [7], [10]–[12].** Therefore, low losses due to reduced OH impurities associated with a higher  $T_g$  would also increase the damage threshold of the fiber compared to TZN fibers.

In this work, we report on the systematic investigation of TZL ternary diagram by performing thermal and optical measurements on bulk glass samples in order to identify appropriate TZL compositions for step-index optical fibers manufacturing. Step-index optical fibers were then drawn from core/cladding preforms and their optical attenuation were characterized.

## 2. Experimental section

### 2.1. Bulk glass preparation

TZL glasses were prepared under room atmosphere by the conventional melt-quenching technique from mixed precursors. **The different glass compositions are specified in Table 1 with the following notation: TZL (resp. TZN) x-y-z for x TeO<sub>2</sub>, y ZnO and z La<sub>2</sub>O<sub>3</sub> (resp. z Na<sub>2</sub>O) in mol%.** Bulk samples of 10g were synthesized using commercial raw materials TeO<sub>2</sub> (Fox Chemicals, 99%), ZnO (Alfa Aesar, 99.99%) and La<sub>2</sub>O<sub>3</sub> (Alfa Aesar, 99.99%) placed in a platinum crucible, then melted at 850°C for 1h in an electric furnace, poured into a brass mold preheated at T<sub>g</sub>-30°C and finally annealed at T<sub>g</sub>-10°C for 4h to remove any residual internal stress induced by the rapid quench of the glass melt. For the TZN composition (80TeO<sub>2</sub>-10ZnO-10Na<sub>2</sub>O, mol.%), there is an additional decarbonation step at 650°C for 30min to remove any residual CO<sub>2</sub> gas from Na<sub>2</sub>CO<sub>3</sub> precursor (Alfa Aesar, 99.5%). After synthesis, the obtained glass plates of 15 x 10 x 5 mm<sup>3</sup> dimensions were finally polished using SiC papers. In a second step, after identification of the most suitable TZL compositions, the glasses were **dehydrated** by manufacturing them in a controlled atmosphere in a glovebox to limit contamination by atmospheric water with higher purity precursors (99.99% for each compound). **The glovebox is under dry air as well as the annealing furnace while the synthesis furnace is placed under pure O<sub>2</sub> ([H<sub>2</sub>O] < 0.5ppm). The glovebox air circulates through H<sub>2</sub>O molecular sieve and a H<sub>2</sub>O sensor to guarantee a dry atmosphere ([H<sub>2</sub>O] < 0.5ppm). The batch size for the controlled atmosphere melts is 40g and corresponds to the batch size used for glasses dedicated to the fiber fabrication. The glass melt is poured in a brass mold to obtain a cylindrical rod with a diameter of 16mm and a length of several centimeters.**

### 2.2. Core-cladding preform preparation and optical fiber drawing

To produce the step-index tellurite glass fibers, the method consists in the combination of two successive steps: Built-in-Casting (BiC) and Rod-in-Tube (RiT) techniques. First, a large-core step-index preform is prepared from two different glasses (core and clad) by BiC as described in [13] and represented on Fig. 1. It is important at this step to carry out a study on the waiting time before removing the excess cladding glass in order to obtain a tube with the smallest possible diameter and the longest possible length. Then, the drawing of this preform allows to obtain 800-μm thin step index canes. Finally, a clad glass rod is mechanically drilled in which the thin clad/core cane is inserted. The obtained preform is then drawn in order to get a small core fiber ( $\Phi_{\text{core}} < 10\mu\text{m}$ ).

The preform drawing is allowed by using a dedicated 3-meters high optical fiber draw tower. The preform was slowly fed into the furnace and the temperature was gradually increased up to ~430°C. The glass was brought to its softening temperature regime while the drawing parameters were continuously monitored to produce the targeted fiber diameter.

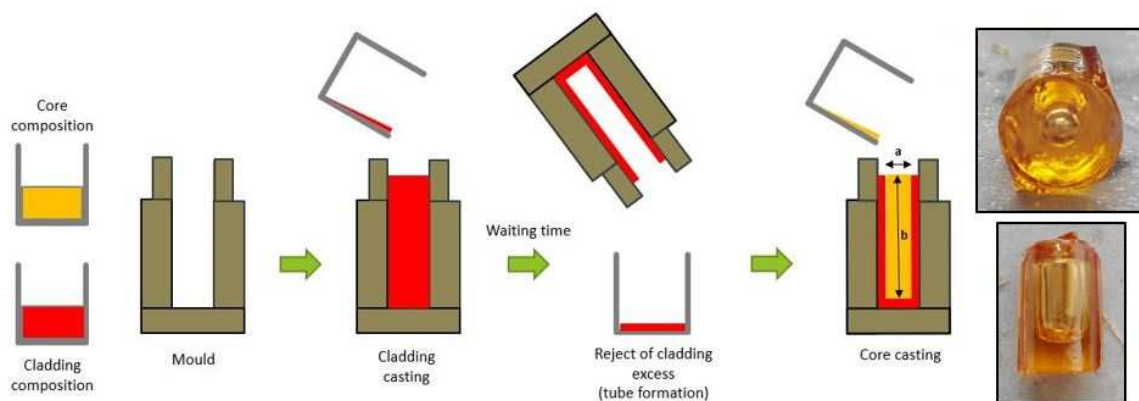


Fig. 1. Core-cladding preform preparation by Built-in-Casting technique

## 2.3. Glass investigation

### 2.3.1. Thermal characterizations

Differential scanning calorimetry (DSC) measurements were performed using a 2920 model TA Instruments apparatus, on small glass pieces sealed into aluminum pans, at a heating rate of 10°C/min, under nitrogen atmosphere. The glass transition temperature was measured as the inflection point of the endothermic baseline deviation.

The linear thermal expansion coefficient of some glass compositions was measured in the range of 150-300°C using a Netzsch 402 PC dilatometer with a heating rate of 10°C/min.

### 2.3.2. Physical characterizations

Totally or partially crystallized glass compositions were studied with an X-ray Bruker D2 Phaser XE-T (CuK $\alpha$  = 1.54184 Å radiation). Diffraction data were collected over the 20-80° 2 $\theta$  range with a 0.02017° step. The crystal phases were then identified using X'Pert High Score Plus software together with the International Centre for Diffraction Data (ICDD) database.

Density measurements were performed using the Archimedes method by weighing a piece of glass in air and then in absolute ethanol. The glass density  $\rho$  can then be calculated as follows (1) [14]:

$$\rho = \frac{A}{A - B} (\rho_L - \rho_0) + \rho_0 \quad (g/cm^3) \quad (1)$$

with A the sample weight in the air, B the sample weight in the absolute ethanol,  $\rho_0$  the air density and  $\rho_L$  the absolute ethanol density adjusted according to the measured temperature.

The oxygen packing density (OPD) was calculated with equation (2) [10] where M is the molecular weight,  $\rho$ , the glass density and C, the number of oxygen atoms for each molecular unit:

$$OPD = 1000 \times C \times \frac{\rho}{M} \quad (mol/L) \quad (2)$$

The molar volume ( $V_m$ ) was calculated using equation (3) [10]:

$$V_m = \frac{M}{\rho} \quad (cm^3/mol) \quad (3)$$

**From  $V_m$ , the molar refraction ( $R_m$ ) was calculated using the Lorentz-Lorenz equation (4) [15]** with n the linear refractive index.  $R_m$  represents the average value of molar refraction for isotropic substances such as glasses.

$$R_m = \frac{n^2 - 1}{n^2 + 2} \times V_m \quad (cm^3/mol) \quad (4)$$

From this equation (4), it is possible to interpret the refractive index evolution as function of  $R_m/V_m$  (5) which represents the spatial optical fill rate [10].

$$n = \sqrt{\frac{2 \left( \frac{R_m}{V_m} \right) + 1}{1 - \left( \frac{R_m}{V_m} \right)}} \quad (5)$$

Finally,  $R_m$  gives access to electronic polarizability ( $\alpha$ ) from relation (6) ( $N_A$ , the Avogadro's number). The electronic polarizability is based on the magnitude of the electrons that respond to an electric field [16].

$$\alpha = \frac{3}{4\pi N_A} \times R_m \quad (\text{Å}^3) \quad (6)$$

### 2.3.3. Optical characterizations

Linear refractive indices were measured on polished glass bulks at several wavelengths (543.5, 632.8, 1064, 1550 nm) using a homemade prism (TiO<sub>2</sub>) coupler refractometer. The measurement error is estimated to be about 10<sup>-3</sup>. The wavelength-dependent refractive index was then determined with the following Sellmeier equation (7) [17] where  $\lambda$  is the wavelength and A, B, and C are the Sellmeier coefficients obtained by a least-square fitting procedure.

$$n^2(\lambda) = A + \frac{B\lambda^2}{\lambda^2 - C^2} \quad (7)$$

The optical basicity concept is based on the Lewis approach. It represents the average electron donor power of the oxide species constituting the medium. The theoretical value of optical basicity ( $\Lambda_{th}$ ) can be calculated by using the equation proposed by Duffy and Ingram [16]. In our case, for a  $x\text{TeO}_2 - y\text{ZnO} - z\text{La}_2\text{O}_3$  [18] composition, the relationship is as follows (8):

$$\Lambda_{th} = x \times \Lambda_{TeO_2}(0.93) + y \times \Lambda_{ZnO}(1.03) + z \times \Lambda_{La_2O_3}(1.07) \quad (8)$$

The UV-visible-near-IR transmission spectra were recorded with a Perkin Elmer Lambda 900 spectrometer on the polished samples whereas mid-IR transmission spectra were recorded with a Fourier transform infrared Perkin-Elmer spectrometer (Spectrum One) on the same samples.

The fiber transmission losses were measured by using the cutback method on several meter lengths of fiber with a Nicolet 6700 Fourier Transform Infrared (FTIR) spectrometer in the 1-4.5  $\mu\text{m}$  range. For the measurement, a halogen lamp emitting from 0.1 to 4.5  $\mu\text{m}$  was used as optical source. The fiber input and output were manually cleaved. The fiber output power was detected using an InSb photodetector.

### 2.3.4. Mechanical characterizations

To compare the mechanical performances of TZL and TZN glasses and fibers, we report here on first mechanical tests. For glass bulks, their Vickers micro-hardness (**HV**) was measured using a Buehler Micromet 2100 Series microhardness apparatus composed of a square-base diamond pyramid with an apical angle of 136°. A load (F) of 25g was applied for a hold-time of 15s. Diagonals length (d) of the indentation was precisely measured at 100x magnification on each glass bulk with a microscope connected to an imaging system. For each composition, values were calculated with the following equation (9) [19] and averaged over eight indentations at different sites on the bulk surface in order to minimize error in the measured hardness. Error bars for this mechanical measurement were evaluated at  $\pm 2.5\%$ .

$$HV (kg_f \cdot mm^{-2}) = \frac{2F \sin\left(\frac{136^\circ}{2}\right)}{9.80665 d^2} = 0.1891 \frac{F}{d^2} \quad (9)$$

Tensile strength measurements give an overview of the maximum uniaxial tensile strength that the fibers can sustain before fracture. The objective, here, was to measure the tensile strength using a Vytran GPX-3000 Series glass fiber processor that allows us to know the range of maximum accepted stress and to compare it for TZN and TZL fibers. For each fiber, the values were averaged over fifteen tests.

## 3. Results and discussion

### 3.1. TZL ternary diagram investigation

In order to find suitable core and clad compositions for the design of step-index fibers, we explored the TZL ternary diagram to determine the vitreous area. For that, in addition to the two binaries (TeO<sub>2</sub>-La<sub>2</sub>O<sub>3</sub> [20] and TeO<sub>2</sub>-ZnO [21]) that have already been studied, several TZL compositions were prepared. Each prepared sample was analyzed by XRD to confirm its amorphous nature and then by DSC to measure its T<sub>g</sub> (Fig. 2). The boundaries of the vitreous domain were determined by the compositions showing distinct diffraction peaks on their XRD pattern (Fig. 2 and 3), characteristic of the presence of crystals within the material.

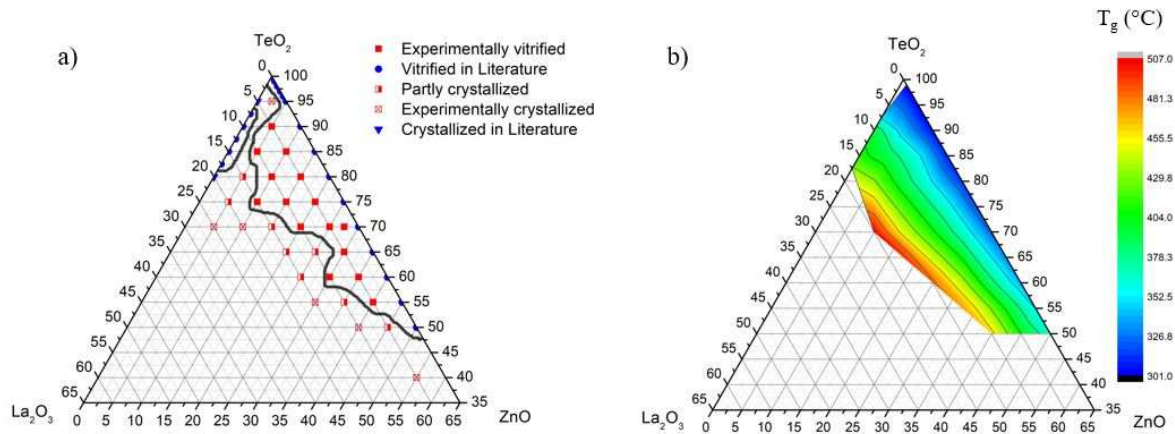


Fig. 2. a: TZL ternary diagram; b: composition influence on the glass transition temperature (Binaries coming from literature: TeO<sub>2</sub>-La<sub>2</sub>O<sub>3</sub> [20] and TeO<sub>2</sub>-ZnO [21])

The first observation that comes from Figs. 2 and 3 is that La<sub>2</sub>O<sub>3</sub> must be introduced into the glassy matrix in limited quantities (< 15 mol.%) to prevent crystallization. Diffractogram of Fig. 3a shows the presence of crystallization peaks for compositions beyond this threshold and the growth of these peaks when the La<sub>2</sub>O<sub>3</sub> concentration increases. Then, the second observation is that the TeO<sub>2</sub> glass forming content must be greater than 55 mol.% to avoid crystallization and depends on the La<sub>2</sub>O<sub>3</sub> content (Fig. 2a and 3b). The crystalline phases corresponding to the major peaks are labelled in Fig. 3. Therefore, in order to ensure a vitreous matrix, the following TZL compositions will be considered:  $x$  TeO<sub>2</sub> – (100- $x$ - $y$ ) ZnO –  $y$  La<sub>2</sub>O<sub>3</sub> with  $x \geq 60$  mol.% and  $0 < y < 15$  mol.%.

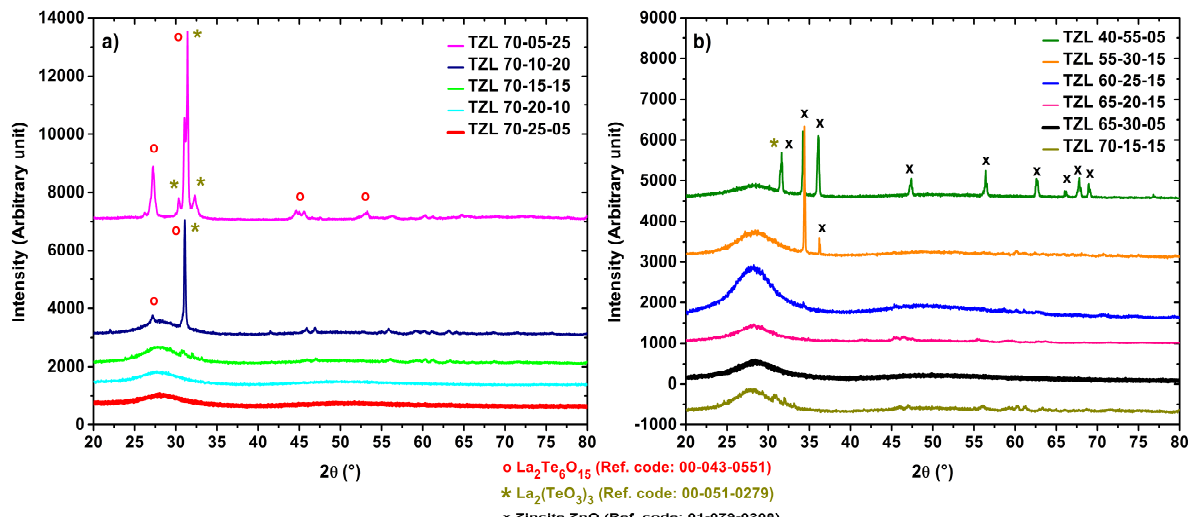


Fig. 3. X-ray diffractograms of TZL samples varying their La<sub>2</sub>O<sub>3</sub> content (a) and TeO<sub>2</sub> content (b) (in bold red and black, the two compositions chosen for optical fibers drawing)

### 3.1.1. Thermal characterizations

The glass transition temperatures  $T_g$  of all the vitreous compositions were measured by DSC and are gathered in Table 1 and Fig. 2b. A strong variation of  $T_g$  is observed in the TZL system (300 to 500°C, see Fig. 2b) which allows a wide range of chemical composition design, in particular when considering multimaterial fibers. Therefore, in order to increase the damage threshold of the fibers, we will be able to select a TZL composition with a higher  $T_g$  compared to the TZN 80-10-10 composition ( $T_g = 285^\circ\text{C}$ ) that is currently used [6]. We also studied the evolution of the samples  $T_g$  as a function of the La<sub>2</sub>O<sub>3</sub> content as well as for a fixed La<sub>2</sub>O<sub>3</sub> content (Fig. 4). Therefore, the  $T_g$  shifts towards high temperatures from 325°C to 449°C with increasing lanthanum content from 0 to 15 mol.% (Fig. 4a). This can be explained by the bond energy of La-O (448.4 kJ.mol<sup>-1</sup>) which is significantly higher than that of Zn-O (350.4 kJ.mol<sup>-1</sup>), and by the modification of the vitreous network. Thermal stability ( $\Delta T = T_x - T_g$  where  $T_x$  is the onset temperature for the first crystallization exothermic peak) is

also found to increase with addition of low  $\text{La}_2\text{O}_3$  content ( $\Delta T_{(\text{TZ } 70-30)} = 98^\circ\text{C}$  vs  $\Delta T_{(\text{TZL } 70-25-05)} = 160^\circ\text{C}$ ). This result is in accordance with the works of Dorofeev *et al.* [8] and Oermann *et al.* [9] who showed that rare earth addition improves tellurite glass stability. For drawing, compositions with a thermal stability higher than  $100^\circ\text{C}$  are empirically preferred to avoid crystallization during the thermal processing. However, as indicated previously, a tendency to crystallization is observed for the samples with 15 mol.% of  $\text{La}_2\text{O}_3$ , indicating that the thermal stability decreases from a certain  $\text{La}_2\text{O}_3$  content. Finally, Fig. 4b shows that at fixed  $\text{La}_2\text{O}_3$  content (5 mol.%), the  $T_g$  tends to slowly increase when  $\text{TeO}_2$  is progressively replaced by  $\text{ZnO}$ . This increase of  $T_g$  upon substitution with  $\text{ZnO}$  in tellurite network ( $\text{ZnO}$  is a glass intermediate, here acting as glass-former) has been already studied in [21]. Furthermore, the thermal stability also increases. Therefore, in the case of TZL compositions with a fixed  $\text{La}_2\text{O}_3$  content of 5 mol.%, we will favor TZL compositions with a  $\text{TeO}_2$  content below 80 mol.%.

**Table 1**

Thermal properties of lanthanum-based tellurite glasses (in bold the compositions which gather both vitrification and drawing criteria)

Compositions (mol. %)	$T_g (\pm 2^\circ\text{C})$	$T_x (\pm 2^\circ\text{C})$	$\Delta T (\pm 4^\circ\text{C})$
<i>Series <math>70\text{TeO}_2-(30-x)\text{ZnO}-x\text{La}_2\text{O}_3</math> (varying <math>\text{La}_2\text{O}_3</math> content)</i>			
TZ 70-30	325	423	98
<b>TZL 70-25-05</b>	<b>365</b>	<b>525</b>	<b>160</b>
<b>TZL 70-20-10</b>	<b>407</b>	-	<b>&gt;100</b>
TZL 70-15-15	449	-	>100
<i>Series <math>(95-y)\text{TeO}_2-y\text{ZnO}-5\text{La}_2\text{O}_3</math> (fixed <math>\text{La}_2\text{O}_3</math> content)</i>			
<b>TZL 60-35-05</b>	<b>385</b>	-	<b>&gt;100</b>
<b>TZL 65-30-05</b>	<b>374</b>	-	<b>&gt;100</b>
<b>TZL 70-25-05</b>	<b>365</b>	<b>525</b>	<b>160</b>
<b>TZL 75-20-05</b>	<b>360</b>	-	<b>&gt;100</b>
TZL 80-15-05	353	510	157
TZL 85-10-05	350	481	131
TZL 90-05-05	343	472	129

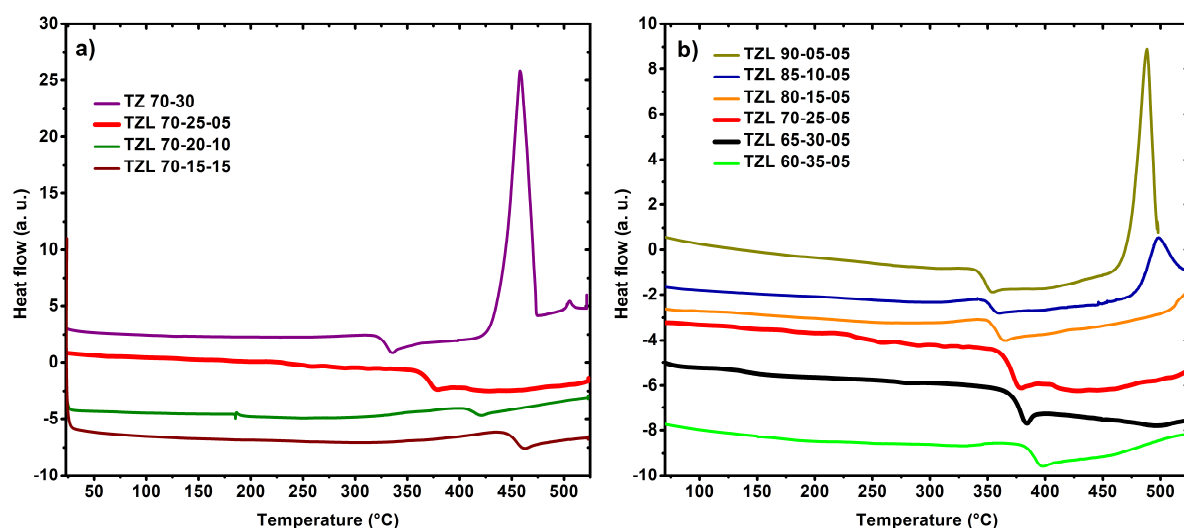


**Fig. 4.** DSC traces of several TZL glasses with a  $\text{La}_2\text{O}_3$  content variation (a) and a fixed  $\text{La}_2\text{O}_3$  content (b). Thermograms were vertically shifted for sake of clarity (in bold red and black, the two compositions chosen for optical fibers drawing)

### 3.1.2. Optical characterizations

Absorption spectra from the UV-visible to the infrared region of the glass samples are shown in Fig. 6. At  $0.48\mu\text{m}$ , we can observe a small shoulder which is due to platinum impurity absorption [22]–[24]. These Pt impurities are responsible for the orange coloration of the glass (Fig. 5) and are introduced during the manufacturing process because of a slight interaction between the glass batch and the platinum crucible. At  $3.3\mu\text{m}$  and  $4.4\mu\text{m}$ , we can identify two absorption peaks relative to the OH species. Fig. 6a shows the influence of  $\text{La}_2\text{O}_3$  content. Both absorption peaks decrease when  $\text{La}_2\text{O}_3$  is introduced into the matrix. Thus, the incorporation of  $\text{La}_2\text{O}_3$  reduces the sensitization to OH species. We also observe a slight increase in the transmission window with the  $\text{La}_2\text{O}_3$  addition (TZ 70-30: optical band gap at  $0.37\mu\text{m}$  and multiphonon absorption cut-off at  $6.20\mu\text{m}$  compared to TZL 70-15-15: optical band gap at  $0.35\mu\text{m}$  and multiphonon absorption cut-off at  $6.29\mu\text{m}$ ). Both limits were determined for an absorption coefficient of  $10\text{cm}^{-1}$ . Fig. 6b shows the absorption spectra at a fixed  $\text{La}_2\text{O}_3$  content. The same observation can be made for the  $\text{TeO}_2$  content decrease. For compositions with low levels of  $\text{TeO}_2$ , the transmission window increases slightly (TZL 60-35-05: optical band gap at  $0.34\mu\text{m}$  and multiphonon absorption cut-off at  $6.24\mu\text{m}$  compared to TZL 90-05-05: optical band gap at  $0.39\mu\text{m}$  and multiphonon absorption cut-off at  $6.20\mu\text{m}$ ). Furthermore, when  $\text{TeO}_2$  content increases with respect to  $\text{ZnO}$  content, we observed a growth of the absorption peak OH.



Fig. 5. Picture of TZL 70-25-05 bulk

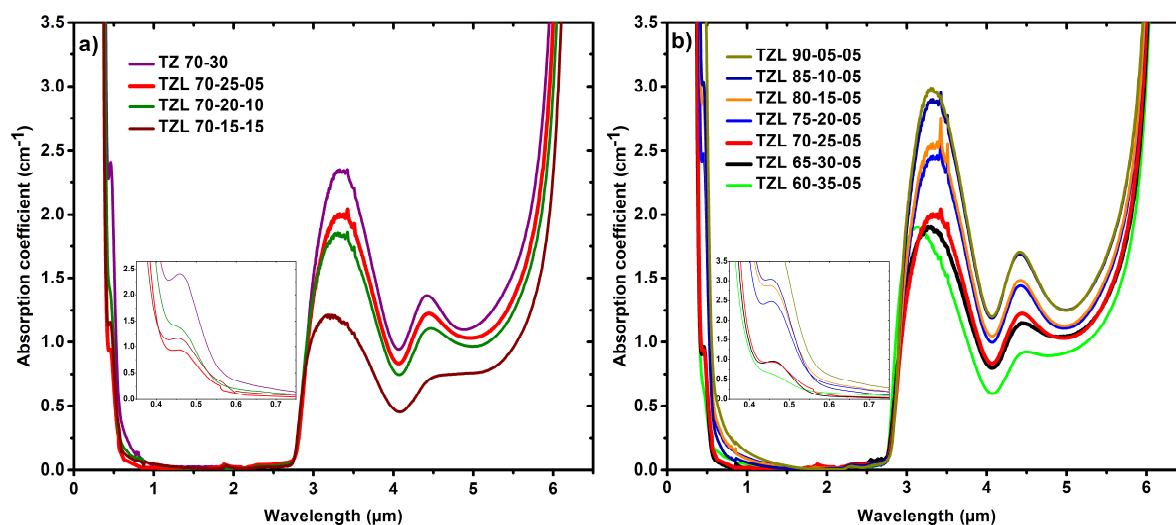


Fig. 6. UV-visible-NIR absorption coefficient spectra of the TZL glass samples as a function of their  $\text{La}_2\text{O}_3$  content (a) and for a fixed  $\text{La}_2\text{O}_3$  content (b) (in bold red and black, the two compositions chosen for optical fibers drawing)

Then, the refractive index of each glass composition was measured, shown in Fig. 7 and gathered in Table 2. The addition of  $\text{La}_2\text{O}_3$  within the glass matrix decreases its refractive index (Fig. 7a). In Fig. 7b, the refractive index evolution of the glasses having the same  $\text{La}_2\text{O}_3$  content is reported. As expected, the refractive index increases as the  $\text{TeO}_2$  content increases with respect to  $\text{ZnO}$  as generally observed with heavy oxides. M.F. Faznny *et al.* [25] who made the same observation on the refractive index evolution with the addition of  $\text{La}_2\text{O}_3$  in a borotellurite matrix, explains this effect by the decreasing number of non-bridging oxygen as the content of lanthanum oxide increases. The wavelength-dependent refractive index is plotted in Fig. 7c and 7d using the Sellmeier equation (7) where  $\lambda$  is the wavelength and A, B and C are the Sellmeier coefficients obtained by a least-square fitting procedure and gathered in Table 3 for each TZL composition.

**Table 2**

Refractive indices as a function of  $\text{La}_2\text{O}_3$  content at 543.5nm, 632.8, 1064nm and 1550nm

Compositions (mol. %)	543.5nm	632.8nm	1064nm	1550nm
<i>Series <math>70\text{TeO}_2-(30-x)\text{ZnO}-x\text{La}_2\text{O}_3</math> (varying <math>\text{La}_2\text{O}_3</math> content)</i>				
TZ 70-30	2.092	2.065	2.024	2.018
TZL 70-25-05	2.068	2.042	2.005	1.999
TZL 70-20-10	2.047	2.023	1.988	1.984
TZL 70-15-15	2.032	2.013	1.977	1.975
<i>Series <math>(95-y)\text{TeO}_2-y\text{ZnO}-5\text{La}_2\text{O}_3</math> (fixed <math>\text{La}_2\text{O}_3</math> content)</i>				
TZL 60-35-05	2.025	2.002	1.968	1.962
TZL 65-30-05	2.047	2.022	1.986	1.980
TZL 70-25-05	2.068	2.042	2.005	1.999
TZL 75-20-05	2.097	2.066	2.026	2.020
TZL 80-15-05	2.115	2.086	2.043	2.037
TZL 85-10-05	2.133	2.105	2.061	2.054
TZL 90-05-05	2.151	2.122	2.077	2.067

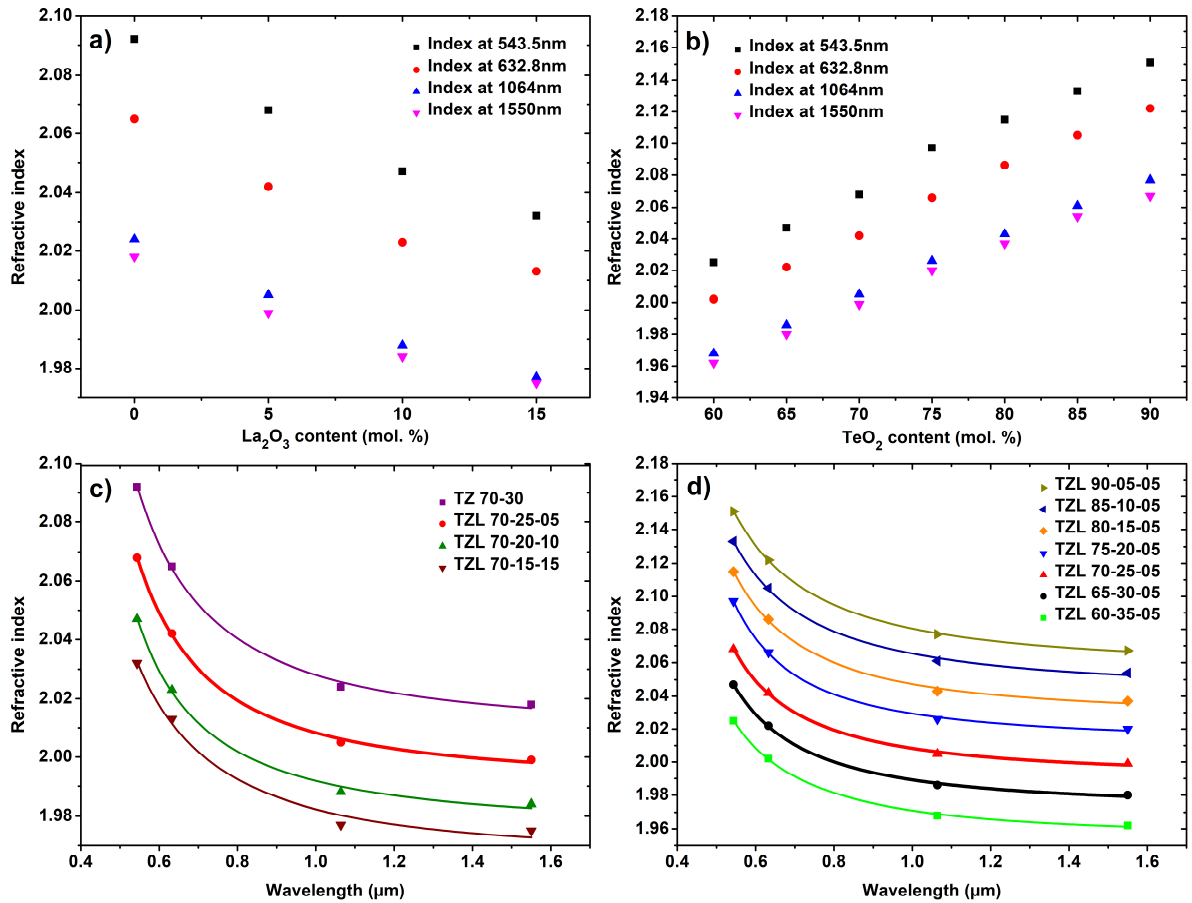


**Fig. 7.** Refractive index as a function of the  $\text{La}_2\text{O}_3$  content variation (a) and at fixed  $\text{La}_2\text{O}_3$  content (b). Wavelength-dependent refractive index with the Sellmeier equation for  $\text{La}_2\text{O}_3$  content variation (c) and at fixed  $\text{La}_2\text{O}_3$  content (d) (**in bold red and black, the two compositions chosen for optical fibers drawing**)

**Table 3**

Sellmeier coefficients obtained by a least-square fitting procedure for each TZL composition

Compositions (mol.%)	A	B	C ( $\mu\text{m}$ )
<i>Series 70TeO<sub>2</sub>-(30-x)ZnO-xLa<sub>2</sub>O<sub>3</sub> (varying La<sub>2</sub>O<sub>3</sub> content)</i>			
TZ 70-30	3.312	0.726	0.307
TZL 70-25-05	3.384	0.583	0.321
TZL 70-20-10	3.417	0.490	0.329
TZL 70-15-15	3.099	0.767	0.275
<i>Series (95-y)TeO<sub>2</sub>-yZnO-5La<sub>2</sub>O<sub>3</sub> (fixed La<sub>2</sub>O<sub>3</sub> content)</i>			
TZL 60-35-05	3.203	0.619	0.303
TZL 65-30-05	3.302	0.590	0.315
TZL 70-25-05	3.384	0.583	0.321
TZL 75-20-05	3.564	0.486	0.351
TZL 80-15-05	3.412	0.701	0.317
TZL 85-10-05	3.257	0.923	0.291
TZL 90-05-05	2.976	1.257	0.266

In order to understand the variation of the glass refractive index upon addition of heavier La<sub>2</sub>O<sub>3</sub> oxide in the network, we have calculated and studied the polarizability, optical basicity and oxygen packing density of the different TZL glasses. All the values are summarized in Table 4. The density of each composition was measured and is reported in Table 4. We observe that as the concentration of La<sub>2</sub>O<sub>3</sub> increases, the density increases too, as expected. This can be explained by the replacement of lighter ZnO oxide with heavier La<sub>2</sub>O<sub>3</sub> oxide. The same behavior is observed, for a fixed La<sub>2</sub>O<sub>3</sub> content. The density increases as ZnO is substituted by heavier TeO<sub>2</sub>.

The oxygen packing density (OPD) corresponds to the oxygen volume concentration in the glass. As the La<sub>2</sub>O<sub>3</sub> content increases at fixed TeO<sub>2</sub> content, the molar volume increases (24,71 to 30,63 cm<sup>3</sup>/mol) and the OPD decreases (68.80 to 65.29 mol.L<sup>-1</sup>), see Fig. 8a. On the other hand, the molar volume (25,65 to 29,15 cm<sup>3</sup>/mol) and the OPD (66.29 to 68.62 mol.L<sup>-1</sup>) increase at fixed La<sub>2</sub>O<sub>3</sub> content with the substitution of ZnO for TeO<sub>2</sub> as shown in Fig. 8b.

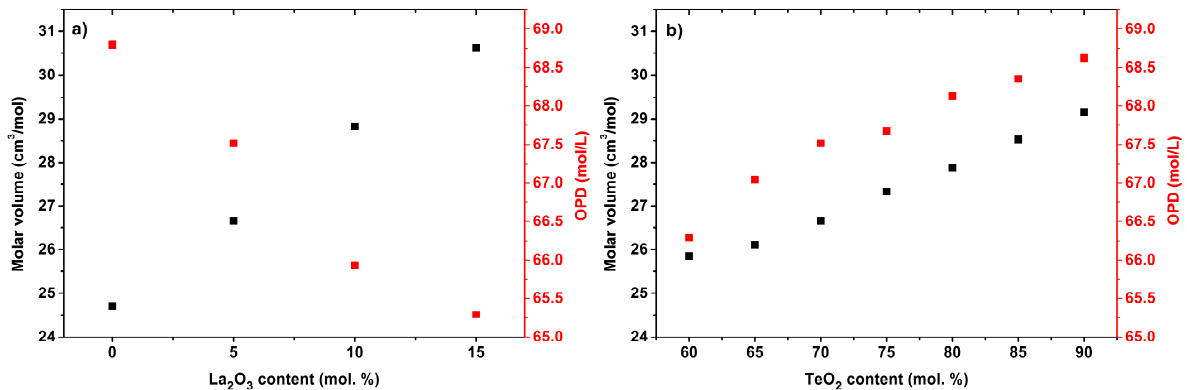


**Fig. 8.** Molar Volume and Oxygen packing density (OPD) of the studied glasses as a function of the La<sub>2</sub>O<sub>3</sub> content (a) and for a fixed La<sub>2</sub>O<sub>3</sub> content (b)

Fig. 9 shows the evolution combining electronic polarizability and linear refractive index at 1.55 $\mu\text{m}$  as a function of the composition. For an increase of La<sub>2</sub>O<sub>3</sub> content (Fig. 9a), while the electronic polarizability increases (together with the molar refraction), the measured refractive index decreases, in accordance with the increase of the molar volume and the related decrease of the OPD. On the other hand, for a fixed La<sub>2</sub>O<sub>3</sub> content and varying the TeO<sub>2</sub>-ZnO ratio (Fig. 9b), we can observe the same trend for the refractive index and the polarizability, the

higher the electronic polarizability, the higher the refractive index, in accordance with the related increase of the OPD, but together with an increase in the molar volume (Fig. 8b).

**Table 4**

Density ( $\rho$ ), molecular weight (M), molar volume ( $V_m$ ), molar refraction ( $R_m$ ), linear refractive index at 1550nm (n), electronic polarizability ( $\alpha$ ), Oxygen packing density (OPD) and optical basicity ( $\Lambda_{th}$ ) of the TZL studied glasses.

Compositions (mol. %)			$\rho$ (g/cm <sup>3</sup> ) ( $\pm 0.002$ )	M (g/mol)	$V_m$ (cm <sup>3</sup> /mol) ( $\pm 0.01$ )	$R_m$ (cm <sup>3</sup> /mol) ( $\pm 0.005$ )	n 1550nm ( $\pm 0.001$ )	$\alpha$ ( $\text{\AA}^3$ ) ( $\pm 0.002$ )	OPD (mol/L) ( $\pm 0.02$ )	$\Lambda_{th}$
TeO <sub>2</sub>	ZnO	La <sub>2</sub> O <sub>3</sub>								
<i>Series 70TeO<sub>2</sub>-(30-x)ZnO-xLa<sub>2</sub>O<sub>3</sub> (varying La<sub>2</sub>O<sub>3</sub> content)</i>										
70	30	0	5.510	136.14	24.71	12.50	2.018	4.96	68.80	0.960
70	25	05	5.565	148.36	26.66	13.32	1.999	5.29	67.52	0.962
70	20	10	5.572	160.58	28.82	14.26	1.984	5.66	65.93	0.964
70	15	15	5.641	172.80	30.63	15.06	1.975	5.97	65.29	0.966
<i>Series (95-y)TeO<sub>2</sub>-yZnO-5La<sub>2</sub>O<sub>3</sub> (fixed La<sub>2</sub>O<sub>3</sub> content)</i>										
60	35	05	5.480	140.54	25.65	12.49	1.962	4.96	66.29	0.972
65	30	05	5.533	144.44	26.11	12.88	1.980	5.11	67.04	0.967
70	25	05	5.565	148.36	26.66	13.32	1.999	5.29	67.52	0.962
75	20	05	5.570	152.27	27.34	13.85	2.020	5.49	67.67	0.957
80	15	05	5.601	156.18	27.88	14.28	2.037	5.66	68.13	0.952
85	10	05	5.612	160.09	28.53	14.77	2.054	5.85	68.35	0.947
90	05	05	5.627	164.00	29.15	15.21	2.067	6.03	68.62	0.942

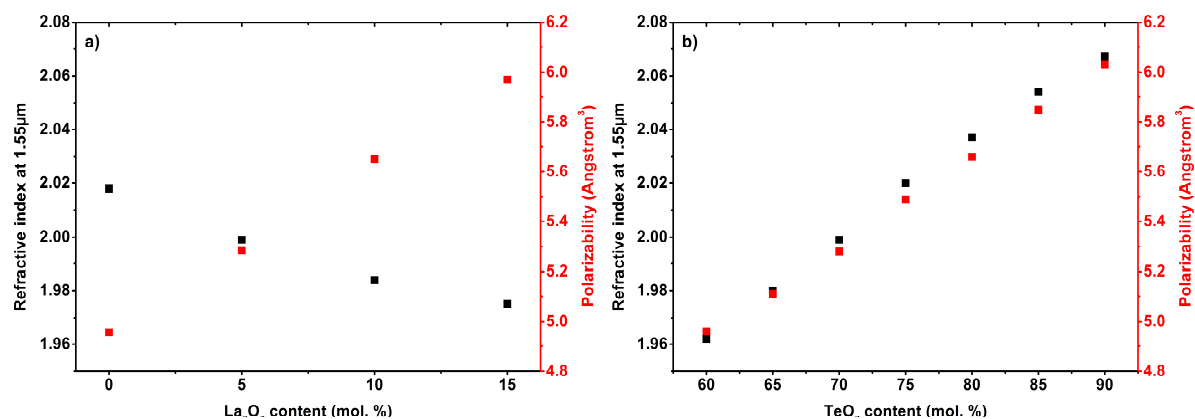


**Fig. 9.** Electronic polarizability and refractive index evolution as a function of La<sub>2</sub>O<sub>3</sub> content variation (a) and at fixed La<sub>2</sub>O<sub>3</sub> content (b)

Fig. 10 presents the variation of the refractive index (at 1.55 μm) and optical basicity as a function of glass composition. The optical basicity  $\Lambda_{th}$  is estimated here from values of oxides optical basicities coming from [26] and related with the oxide ions polarizability calculated for  $n_D$  (note that the trend of refractive index variation with the composition is the same, whatever the wavelength at which the refractive index is measured (Fig. 7)). In this case, the contribution of the cations polarizability is subtracted from the glass polarizability to obtain the oxide ions polarizability. From this  $\Lambda_{th}$  estimation, we observe that, whatever the variation in the glass composition, the variation of the optical basicity calculated in this way is in opposite trend with the variation of the refractive index when this evolution should be related to the glass refractive index variation since optical basicity is linked to the magnitude of negative charge borne by the oxygen atoms or ions and finally to their polarizability [27]. Therefore, as a first approximation, the contribution of cations is neglected in predicting the evolution of the refractive index. However, here, Te(+IV) has an important, non-negligible polarizability and its effect on the oxide ions polarizability can no more be neglected. What's more, depending on the tellurium oxide

polyhedrons involved in the glass composition ( $\text{TeO}_4^\circ$ ,  $\text{TeO}_4^-$ ,  $\text{TeO}_3^-$ ,  $\text{TeO}_3^{2-}$ ), their relative optical basicity is significantly different, varying from 0.82 to 1.23 [28]. Thus, to reach in our compositions an optical basicity which would be representative of the refractive index variation, it should be necessary to perform a structural study (Raman study for instance) to identify the relative importance of the different  $[\text{Te}_x\text{O}_y]$  polyhedrons present in our glass composition. Fig. 11 gathers all these results and present the variation of the different studied parameters ( $V_m$ , OPD,  $\alpha$ ,  $\Lambda$  and  $n$ ) as a function of composition for a varying  $\text{La}_2\text{O}_3$  amount (Fig. 11a) and at a fixed  $\text{La}_2\text{O}_3$  amount (Fig. 11b). From these different results and for these compositions, the OPD parameter is finally the simplest way to predict the refractive index variation (Fig. 11a and b). Finally, by plotting the refractive index as a function of the spatial optical fill rate ( $R_m/V_m$ ) (Fig. 11c), the overall compositions are on a same line with an increase in the refractive index and the  $R_m/V_m$  ratio when the  $\text{TeO}_2$  content increases and a decrease in the refractive index and the  $R_m/V_m$  ratio when the  $\text{La}_2\text{O}_3$  content increases. Using this graph, it is thus possible to predict and anticipate the refractive index of a new TZL composition. One can note that we can also plot the refractive index as a function of  $R_m \times \text{OPD} = (R_m/V_m) \times C \times 10^3$  (Fig. 11d). This parameter represents a ponderation of the molar refraction by the oxygen packing density, and allows to distinguish between the two series of glasses, at fixed or variable  $\text{La}_2\text{O}_3$  content (resp. variable or fixed  $\text{TeO}_2$  content)

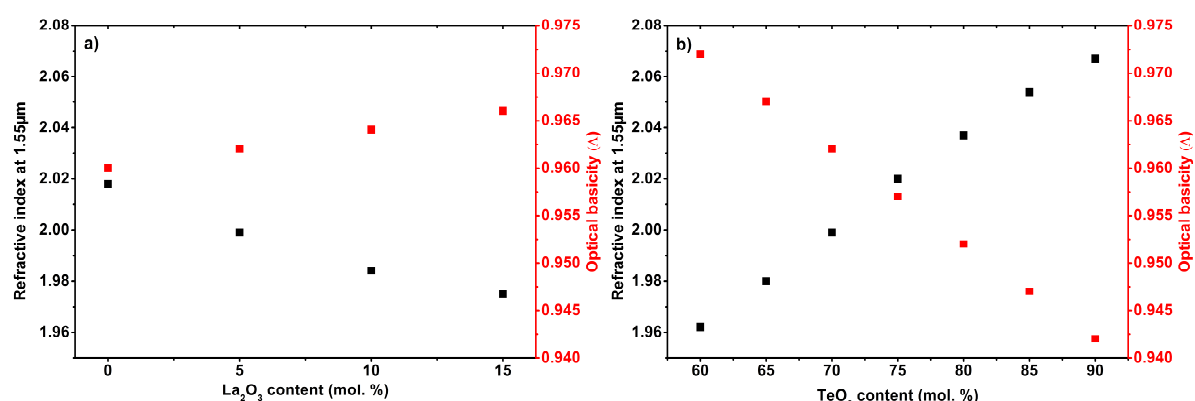


Fig. 10. Optical basicity ( $\Lambda$ ) and refractive index evolution as a function of  $\text{La}_2\text{O}_3$  content variation (a) and at fixed  $\text{La}_2\text{O}_3$  content (b)

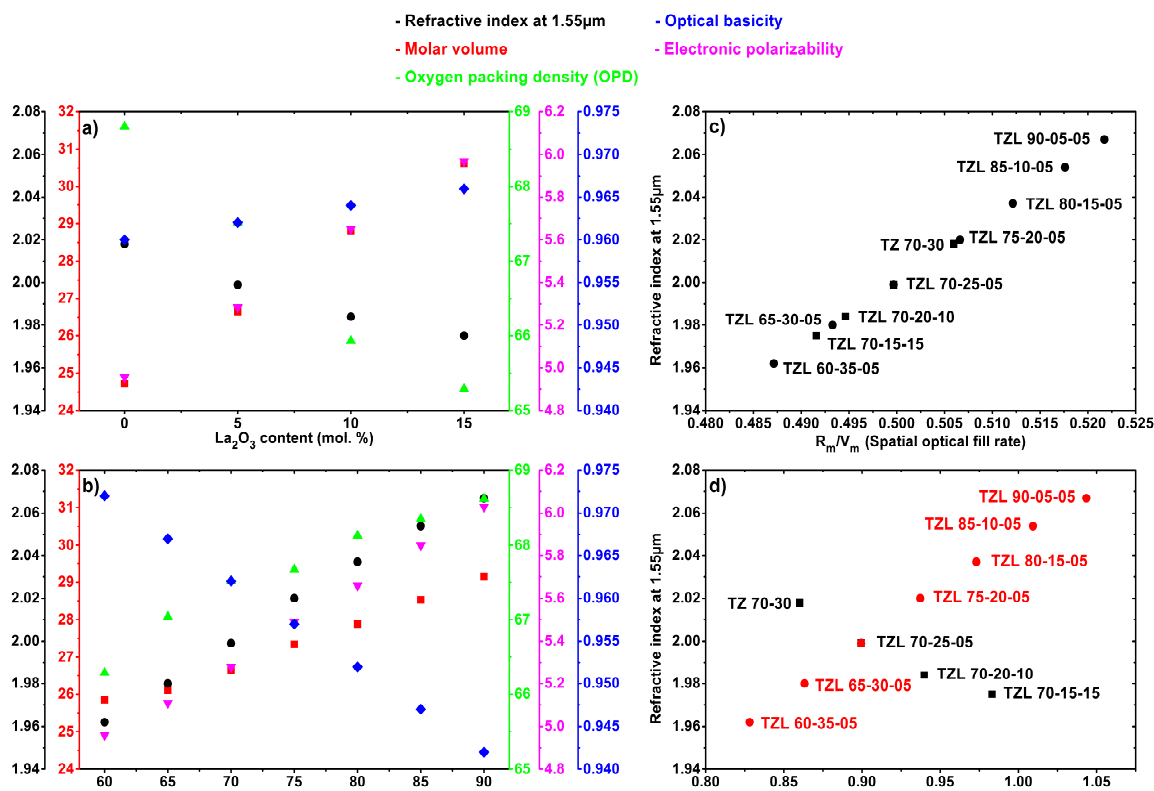


Fig. 11. Molar volume, linear refractive index at  $1.55\mu\text{m}$ , electronic polarizability, Oxygen packing density (OPD) and optical basicity ( $\Lambda$ ) of the TZL studied glasses as a function of their  $\text{La}_2\text{O}_3$  content (a) and for a fixed  $\text{La}_2\text{O}_3$  content ( $\text{TeO}_2$  content variation) (b). Evolution of the refractive index at  $1.55\mu\text{m}$  as a function of the spatial optical fill rate  $R_m/V_m$  for each TZL composition (c) and as a function of  $R_m \times \text{OPD}$  (d)

### 3.2. Cladding and core selections for step-index optical fibers manufacturing

Two glass compositions were selected from the above study of TZL vitreous system for the fabrication of step-index optical fibers, by taking into account their close thermal and thermo-mechanical properties, as well as their optical properties to ensure light guiding into the fiber. For the fiber core, the selected glass composition is 70TeO<sub>2</sub> - 25ZnO - 05La<sub>2</sub>O<sub>3</sub> (mol.%) whereas for the fiber cladding, it is 65TeO<sub>2</sub> - 30ZnO - 05La<sub>2</sub>O<sub>3</sub>. **We have chosen a core glass composition with 5 mol. % of La<sub>2</sub>O<sub>3</sub> for a question of stability of the core vitreous material in relation to the fiber drawing process. This composition has the advantage to exhibit a strong thermal stability (T<sub>x</sub>-T<sub>g</sub>) of 160°C. As the temperature of the glass is raised between T<sub>g</sub> and T<sub>x</sub> during the fiber drawing process, it is essential that this difference (T<sub>x</sub>-T<sub>g</sub>) is as large as possible in order to avoid the risk of crystallization during the fiber drawing process. The clad composition (TZL 65-30-05) was then chosen with a T<sub>g</sub> and a refractive index compatible with the fiber drawing process. Their thermal and optical properties are summarized up in Table 5 and represented in bold red and black plots on Figs. 3, 4, 6 and 7.** From a thermal and thermo-mechanical point of view, these compositions exhibit close glass transition temperature for the drawing and similar thermal expansion coefficients (TEC) which would allow to avoid any fracture and ensuring good cohesion of the assembly. From an optical point of view, refractive indices were chosen to ensure the light confinement in the core of the fiber with a core refractive index higher than the cladding refractive index with an index difference greater than 10<sup>-2</sup>. This optical fiber is monomodal (Normalized frequency (10) [29]: V < 2.405) from 2.6μm for a core radius “a” of 3.5μm. The numerical aperture of the fiber is around 0.27.

$$V = 2\pi a \sqrt{\frac{n_{core}^2 - n_{cladding}^2}{\lambda}} \quad (10)$$

**Table 5**  
Thermal and optical properties for the selected core and cladding composition

Composition (mol%)	T <sub>g</sub> (°C)	T <sub>x</sub> (°C)	ΔT (°C)	TEC (°C <sup>-1</sup> )	n (1.55μm)
<b>TZL 70-25-05 (core)</b>	365	525	160	1.143 x 10 <sup>-5</sup>	1.999
<b>TZL 65-30-05 (clad)</b>	374	-	>100	1.025 x 10 <sup>-5</sup>	1.980

The optical fibers were manufactured using a combination of Built-in-casting (BiC) and Rod-in-tube (RiT) techniques as described above in section 2.2. These fibers were hand cleaved and observed under an optical microscope to check the core-clad interface quality and the core diameter as shown in Fig. 12.

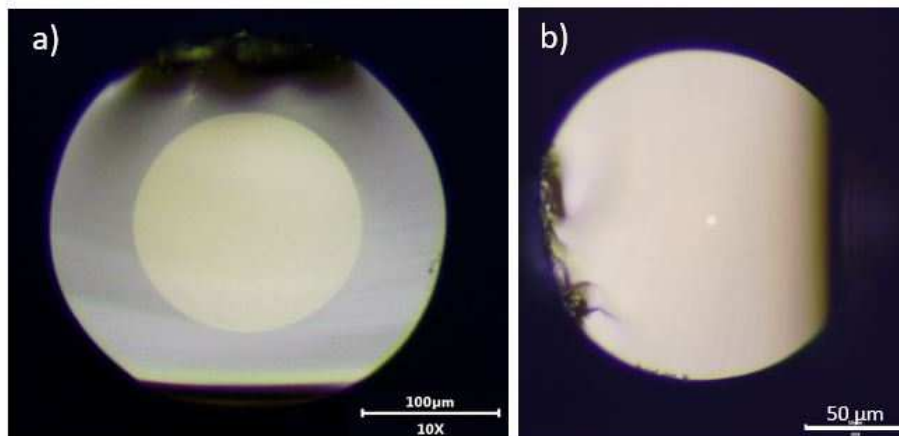


**Fig. 12.** Optical micrographs of different fibers cleaves: a) 170μm core fiber diameter obtained with the large-core preform resulting from the BIC method and b) small-core fiber (7μm core diameter) prepared through the RiT method

The optical losses of these fibers were then measured by the cut-back technique, see Fig. 13b (black line). This fiber transmits light up to 2.7μm and has a minimum loss of 2.85 dB/m at 1.4μm. The transmission and losses of these fibers can be improved in future work by **dehydrating** the glasses with a synthesis in a controlled

atmosphere and by the use of precursors with a better chemical quality in order to limit contamination by water and transition metals that lead to parasitic absorption [23], [30].

In view of replacing the well-known TZN glasses by these promising TZL glasses for the manufacturing of glass-metal hybrid optical fibers or their use in the generation of supercontinuum, we compared the transmission (Fig. 13a) and the fibers losses (Fig. 13b) of the selected core composition (TZL 70-25-05) with the former one (TZN 80-10-10) which was used previously. Both bulks and preforms were prepared at room atmosphere without any purification process and using the same quality for the precursors. Both glasses are limited by the multiphonon absorption which appears around  $6.25\mu\text{m}$ . However, OH absorptions at  $3.3\mu\text{m}$  and  $4.4\mu\text{m}$  are more pronounced for the TZN 80-10-10 composition. It can therefore be assumed that this composition is more sensitive to atmospheric OH-contamination which significantly alters not only the optical properties but also probably the mechanical properties. **Several reasons can explain this fact. Based on the drawing temperature which is higher for TZL glass compared to TZN, we assume that the TZL viscosity is higher than the TZN one at the synthesis temperature, fixed at  $850^\circ\text{C}$  for both glasses. This higher viscosity might prevent water diffusion from the atmosphere to the melt, but could also on the other hand prevent OH removal from the melt. The starting product  $\text{Na}_2\text{CO}_3$  used for TZN may also bring water in the melt. Another parameter, as previously stated, which could also explain this TZN higher sensitivity to water, is that the incorporation of  $\text{Na}_2\text{O}$  in the glass composition leads to non-bridging oxygens and increases the basicity of the glass melt, thus increasing reactivity with water [10]–[12].** The optical losses of fibers drawn from air-cast glasses confirm the better transmission of TZL fiber vs TZN fibers, even if of course the IR transmission is limited by OH absorption (Fig. 13b). TZL 70-25-05 and TZN 80-10-10 glasses were also synthesized with higher purity precursors in a glovebox-controlled atmosphere to limit contamination by atmospheric water (Fig. 13a) and compared, to estimate the potential of TZL 70-25-05 for low losses optical fibers (Fig. 13b). We can observe in Fig. 13a the strong decrease of OH absorption peaks for each glass but the purification of TZL is more efficient thanks to the low sensitivity to OH contamination as we indicated above. In this way, this strong decrease allows us to lower the optical losses of the fiber down to less than  $2\text{dB/m}$  up to  $2.75\mu\text{m}$  for TZL fibers and  $2.65\mu\text{m}$  for TZN fibers with a minimum loss of  $1.25\text{dB/m}$  at  $2.15\mu\text{m}$  for TZL fibers (Fig. 13b). However, for TZN fibers, the remaining OH content ends up the fiber transmission at  $2,8\mu\text{m}$  while for TZL fiber, the transmission extends above  $3\mu\text{m}$  and illustrates the superior behavior of TZL glasses regarding OH contamination, even if the OH-groups are not totally removed. **A systematic study of purification and dehydration process of TZL glasses is currently in progress.**

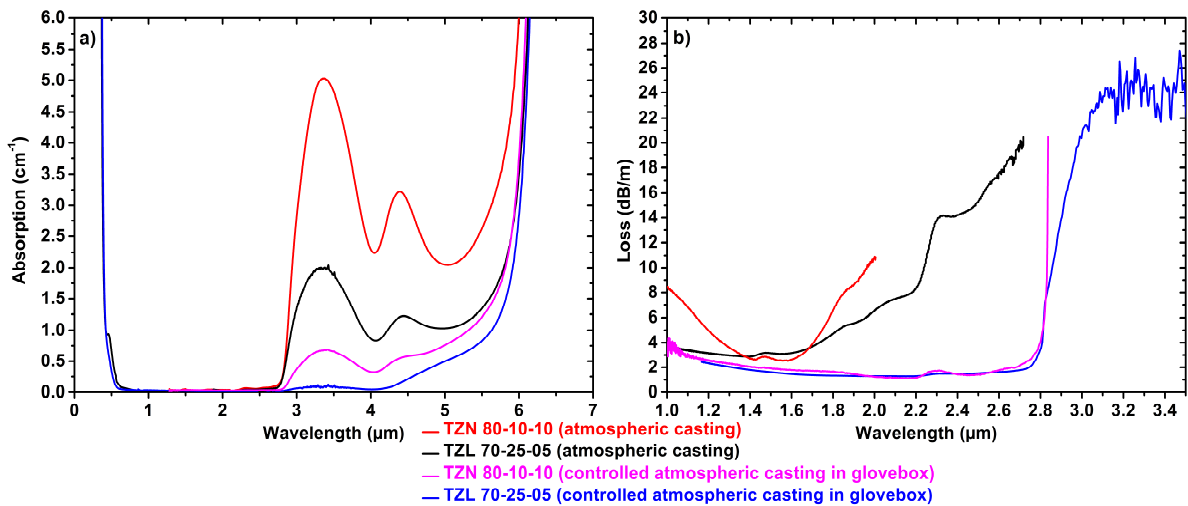


Fig. 13. a) Absorption coefficient spectra of TZL 70-25-05 and TZN 80-10-10 core glasses cast in air and in glovebox. b) Comparison of losses obtained for corresponding step index fibers.

### 3.3. Mechanical characterizations

TZL fibers appear to be mechanically stronger and easier to handle compared to TZN fibers, in particular to crushing. To verify this fact, first mechanical tests were performed such as micro-hardness measurements on the bulks and tensile strength measurements on the fibers. The results are summarized in Table 6. Micro-hardness measurements provide interesting information on the material's behavior to surface damage (Fig. 14). The average Vickers hardness increases by about 35% from  $2.04\text{ GPa}$  to  $2.73\text{ GPa}$  when switching from TZN 80-10-10 to TZL 70-25-05. However, in our case, the synthesis atmosphere in which the glass is prepared does not

seem to have a significant influence on the hardness value (2.73 GPa for atmospheric casting vs 2.68 GPa for controlled atmospheric casting in glovebox). On the other hand, for tensile strength measurements, the maximum mechanical tensile stress also increases by about 140% from 37 MPa to 89 MPa between TZN 80-10-10 and TZL 70-25-05 fibers. These preliminary mechanical measurements confirm the superior mechanical behavior of TZL glasses and fibers, which will be now studied more in details, by measuring these mechanical parameters for the different glass compositions, and especially by studying the tensile strength of fibers drawn from glasses casted in controlled atmosphere.

**Table 6**  
Vickers hardness of several TZN and TZL glasses on bulk and maximum mechanical tensile stress for corresponding fibers

Composition (mol%)	Vickers Hardness (GPa)	Maximum mechanical tensile stress (MPa)
TZN 80-10-10 (atmospheric casting)	2.04	37
TZL 70-25-05 (atmospheric casting)	2.73	89
TZL 70-25-05 (controlled atmospheric casting in glovebox)	2.68	-

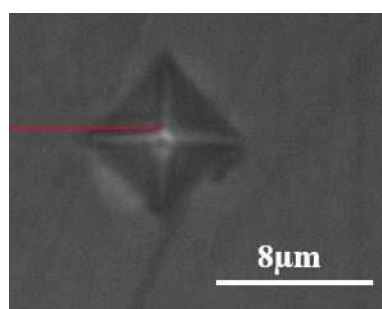


**Fig. 14.** Indentation trace on TZL 70-25-05 bulk after micro-hardness testing

#### 4. Conclusions

The  $\text{TeO}_2\text{-ZnO-La}_2\text{O}_3$  ternary glass system has been fully explored in order to select appropriate compositions for the fabrication of step-index optical fibers. For this purpose,  $70\text{TeO}_2\text{-(30-x)ZnO-xLa}_2\text{O}_3$  series (varying  $\text{La}_2\text{O}_3$  content) and  $(95-y)\text{TeO}_2\text{-yZnO-5La}_2\text{O}_3$  series (fixed  $\text{La}_2\text{O}_3$  content) were prepared and characterized thermally and optically to understand the influence of the  $\text{La}_2\text{O}_3$  content on the physical properties of the glass. A study of the relationship between refractive index and glass physical parameters has been conducted. Compared to the TZN 80-10-10 composition, the selected TZL 70-25-05 core composition has a higher  $T_g$  which will allow in particular to increase the threshold damage of the fibers and improve the metal-glass interface quality for the hybrid optical fibers [31]. In addition, TZL glasses have the advantage to present better mechanical properties with an improved hardness and tensile strength which allow an easier handling of TZL fibers compared to TZN fibers. To complete this study, additional mechanical measurements are being investigated to be presented to the glass community. Moreover, in order to reach a better understanding of the glass structure and of the relationship between the refractive index, the molar volume and the electronic polarizability as a function of the glass composition, an in-depth Raman structural study is in progress. Lastly, these glasses were also subjected to **a purification and dehydration study** to limit contamination from transition metals and water in the atmosphere. To do this, the glasses were prepared under controlled atmosphere in a glovebox with 5N precursors and other compounds designed to capture OH species and remove them from the final glass matrix. **The improvement of the optical properties and the impact of the purification and dehydration processes are currently under further investigation.**

#### Acknowledgements

This research is the result of a collaboration between the Laboratoire Interdisciplinaire Carnot de Bourgogne in Dijon in France supported by the French National Research Agency (ANR-17-CE08-0042-04, PROTEus project) and the Centre d'Optique, Photonique et Laser in Quebec City in Canada supported by the Canadian

Excellence Research Chair Program (CERC) in Photonics Innovations and the Natural Sciences and Engineering Research Council of Canada (NSERC). We are also grateful to acknowledge the Council of the French Region Bourgogne Franche-Comté and the European program FEDER.  
This work has also been supported by the EIPHI Graduate School (contract ANR-17-EURE-0002).

## References

- [1] R. A. H. El-Mallawany, "Tellurites Glasses Handbook," Physical Properties and Data, Second Edition, CRC Press Taylor & Francis Group, 2012.
- [2] V. A. G. Rivera, D. Manzani, and V. A. G. Rivera, *Technological Advances in Tellurite Glasses*. Springer, 2017.
- [3] D. L. Rhonehouse *et al.*, "Low loss, wide transparency, robust tellurite glass fibers for mid-IR (2-5  $\mu\text{m}$ ) applications," in *Technologies for Optical Countermeasures X; and High-Power Lasers 2013: Technology and Systems*, 2013, vol. 8898, p. 88980D.
- [4] R. Wang, X. Meng, F. Yin, Y. Feng, G. Qin, and W. Qin, "Heavily erbium-doped low-hydroxyl fluorotellurite glasses for 2.7  $\mu\text{m}$  laser applications," *Optical Materials Express*, vol. 3, no. 8, pp. 1127–1136, 2013.
- [5] P. Froidevaux *et al.*, "Dispersion-engineered step-index tellurite fibers for mid-infrared coherent supercontinuum generation from 1.5 to 4.5  $\mu\text{m}$  with sub-nanojoule femtosecond pump pulses," *Applied Sciences*, vol. 8, no. 10, p. 1875, 2018.
- [6] C. Strutynski *et al.*, "Tellurite-based core-clad dual-electrodes composite fibers," *Optical Materials Express*, vol. 7, no. 5, pp. 1503–1508, 2017.
- [7] D. L. Rhonehouse *et al.*, "Low-loss UV to mid IR optical tellurium oxide glass and fiber for linear, non-linear and active devices.," US Patent 8,805,133, August 12 2014.
- [8] V. V. Dorofeev *et al.*, "High-purity TeO<sub>2</sub>-WO<sub>3</sub>-(La<sub>2</sub>O<sub>3</sub>, Bi<sub>2</sub>O<sub>3</sub>) glasses for fiber-optics," *Optical Materials*, vol. 33, no. 12, pp. 1911–1915, 2011.
- [9] M. R. Oermann, H. Ebendorff-Heidepriem, Y. Li, T.-C. Foo, and T. M. Monro, "Index matching between passive and active tellurite glasses for use in microstructured fiber lasers: Erbium doped lanthanum-tellurite glass," *Optics express*, vol. 17, no. 18, pp. 15578–15584, 2009.
- [10] H. Scholze, *Glass: nature, structure, and properties*. Springer Science & Business Media, 2012.
- [11] W. H. Zachariasen, "The atomic arrangement in glass," *Journal of the American Chemical Society*, vol. 54, no. 10, pp. 3841–3851, 1932.
- [12] W. H. Zachariasen, "The vitreous state," *The Journal of Chemical Physics*, vol. 3, no. 3, pp. 162–163, 1935.
- [13] C. Strutynski *et al.*, "Fabrication and characterization of step-index tellurite fibers with varying numerical aperture for near- and mid-infrared nonlinear optics," *JOSA B*, vol. 33, no. 11, pp. D12–D18, 2016.
- [14] E. Hecht, *Physique*. De Boeck Supérieur, 1999.
- [15] V. Dimitrov and S. Sakka, "Electronic oxide polarizability and optical basicity of simple oxides. I," *Journal of Applied Physics*, vol. 79, no. 3, pp. 1736–1740, 1996.
- [16] J. A. Duffy and M. D. Ingram, "An interpretation of glass chemistry in terms of the optical basicity concept," *Journal of Non-Crystalline Solids*, vol. 21, no. 3, pp. 373–410, 1976.
- [17] J. Zarzycki, *Les verres et l'état vitreux*. Masson, 1982.
- [18] A. Leboutteiller and P. Courtine, "Improvement of a bulk optical basicity table for oxidic systems," *Journal of Solid State Chemistry*, vol. 137, no. 1, pp. 94–103, 1998.
- [19] J. Barton and C. Guillemet, "Le verre," *Science et Technologie, EDP Sciences*, 2005.
- [20] R. El-Mallawany, A. Abdel-Kader, M. El-Hawary, and N. El-Khoshkhany, "Volume and thermal studies for tellurite glasses," *Journal of materials science*, vol. 45, no. 4, pp. 871–887, 2010.
- [21] N. S. Tagiara, D. Palles, E. D. Simandiras, V. Psycharis, A. Kyritsis, and E. I. Kamitsos, "Synthesis, thermal and structural properties of pure TeO<sub>2</sub> glass and zinc-tellurite glasses," *Journal of Non-Crystalline Solids*, vol. 457, pp. 116–125, 2017.
- [22] F. Désévéday *et al.*, "Review of tellurite glasses purification issues for mid-IR optical fiber applications," *Journal of the American Ceramic Society*, vol. 103, no. 8, pp. 4017–4034, 2020.
- [23] M. F. Churbanov, A. N. Moiseev, A. V. Chilyasov, V. V. Dorofeev, and I. A. Kraev, "Production of high-purity TeO<sub>2</sub>-ZnO and TeO<sub>2</sub>-WO<sub>3</sub> glasses with the reduced content of OH-groups," *Journal of Optoelectronics and Advanced Materials*, vol. 9, no. 10, pp. 3229–3234, 2007.
- [24] I. Savellii, "Fibres optiques à coeur suspendu en verre d'oxyde de tellure et génération d'effets non linéaires dans l'infrarouge au-delà de 2 microns," 2012.
- [25] M. F. Faznny, M. K. Halimah, and M. N. Azlan, "Effect of lanthanum oxide on optical properties of zinc borotellurite glass system," *Journal of Optoelectronics and Biomedical Materials*, vol. 8, no. 2, pp. 49–59, 2016.
- [26] T. Honma, Y. Benino, T. Fujiwara, T. Komatsu, R. Sato, and V. Dimitrov, "Electronic polarizability, optical basicity, and interaction parameter of La<sub>2</sub>O<sub>3</sub> and related glasses," *Journal of applied physics*, vol. 91, no. 5, pp. 2942–2950, 2002.
- [27] J. A. Duffy, "Optical basicity: A practical acid-base theory for oxides and oxyanions," *Journal of chemical education*, vol. 73, no. 12, p. 1138, 1996.
- [28] V. Dimitrov, "Communication: Group optical basicity of tellurite glasses," *Physics and Chemistry of Glasses-European Journal of Glass Science and Technology Part B*, vol. 52, no. 3, pp. 138–141, 2011.
- [29] A. Méndez and T. F. Morse, *Specialty optical fibers handbook*. Elsevier, 2011.
- [30] V. V. Dorofeev *et al.*, "Production and properties of high purity TeO<sub>2</sub>- WO<sub>3</sub>-(La<sub>2</sub>O<sub>3</sub>, Bi<sub>2</sub>O<sub>3</sub>) and TeO<sub>2</sub>- ZnO- Na<sub>2</sub>O- Bi<sub>2</sub>O<sub>3</sub> glasses," *Journal of non-crystalline solids*, vol. 357, no. 11–13, pp. 2366–2370, 2011.

- [31] A. Maldonado *et al.*, “Elaboration of multimaterials optical fibers combining tellurite glass and metal for electro-optical applications,” in *Fiber Lasers and Glass Photonics: Materials through Applications II*, 2020, vol. 11357, p. 113570U.